minerals

MDPI

Article

Middle-Late Eocene Climate in the Pearl River Mouth Basin: Evidence from a Palynological and Geological Element Record in the Xijiang Main Subsag

Guangrong Peng [1], Weitao Chen [1], Peimeng Jia [1], Ming Luo [1], Ye He [1], Yaoyao Jin [1], Chuan Xu [2] and Xuanlong Shan [2,*]

[1] Shenzhen Branch of CNOOC, Ltd., Shenzhen 518000, China
[2] College of Earth Sciences, Jilin University, Changchun 130061, China
* Correspondence: shanxl@jlu.edu.cn

Abstract: The temperature changes in the middle-late Eocene had a profound impact on various ecosystems around the world. This has been confirmed not only in marine sediments but also in lake ecosystems, which have provided more detailed isochronous continental sedimentary records. Based on systematic palynological and element analyses of fine-grained lacustrine sediments from the Xijiang main subsag in the Pearl River Mouth Basin, southern China, we reconstructed the climate evolution of the middle-late Eocene. A total of 73 genera and 115 species of sporopollen fossils were identified from the middle-late Eocene in the study area. Three pollen zones comprising *Quercoidites–Polypodiaceaesporites–Pinuspollenites*, *Pinuspollenites–Ulmipollenites–Cedripites*, and *Pinuspollenites–Abietineaepollenites–Juglanspollenites* were established from bottom to top. The analysis of the vegetation types, climatic zones, and dry–humid types of the sporopollen showed that, in the study area, the Eocene was dominated by a subtropical–warm temperate climate: the early-late Eocene was dominated by a temperate climate, and the late Eocene was characterized by the prevalence of a warm temperate climate, which was consistent with the palaeoclimate reconstruction results for element geochemical indices (Fe/Mn, Sr/Cu, CIA, PIA, etc.). In addition, the comparative study showed that the middle-late Eocene in the study area was characterized by a warm and humid climate, which transitioned to a warm and cool semihumid–semiarid climate and then a warm and cool semihumid climate. These findings demonstrated a good coupling relationship with the trend for the changes in the global palaeotemperature and can be used as an isochronous continental sedimentary response.

Keywords: Pearl River Mouth Basin; Xijiang main subsag; middle-late Eocene; palynological record; element geochemistry; palaeoclimate

check for updates

Citation: Peng, G.; Chen, W.; Jia, P.; Luo, M.; He, Y.; Jin, Y.; Xu, C.; Shan, X. Middle-Late Eocene Climate in the Pearl River Mouth Basin: Evidence from a Palynological and Geological Element Record in the Xijiang Main Subsag. *Minerals* **2023**, *13*, 374. https://doi.org/10.3390/min13030374

Academic Editor: Hermann Kudrass

Received: 18 December 2022
Revised: 3 March 2023
Accepted: 3 March 2023
Published: 8 March 2023

Copyright: © 2023 by the authors. Licensee MDPI, Basel, Switzerland. This article is an open access article distributed under the terms and conditions of the Creative Commons Attribution (CC BY) license (https://creativecommons.org/licenses/by/4.0/).

1. Introduction

From integrating studies at global and regional scales, it is evident that the Palaeogene climate was warmer and wetter than the present climate [1,2]. Although the Palaeogene is known for its typical greenhouse climate, it is also widely accepted that the global climate underwent several rapid and long-term changes during this period, from hot chamber to greenhouse and from greenhouse to cold chamber, which had an important impact on the evolution of global palaeoecosystems [3–5]. The extreme climate events of the Palaeogene (Palaeocene–Eocene thermal maximum (PETM), Eocene thermal maximum (ETM), early Eocene climate optimization (EECO), and Eocene–Oligocene transition (EOT)) have been extensively studied [6–9]. The carbon and nitrogen cycling mechanisms, organic carbon burial, marine circulation and extinction, and succession and migration phenomena are well-constrained in marine and terrestrial systems for these events [10,11]. Compared with the strong interest in extreme climate events, the understanding of the greenhouse climate in the middle-late Eocene is slightly weak. To date, research has mostly focused on

marine sediments in the middle-late Eocene, while the continental sedimentary response has not received enough attention. Relevant reports have appeared sporadically around the world [12,13]. Therefore, there is an urgent need for more middle-late Eocene terrestrial sedimentary records to deepen our understanding of the middle-late Eocene climate and ecological environment.

In response to changes in altitude, latitude, and climate, vegetation often exhibits rapid succession and migration, so vegetation types can be used as sensitive temperature indicators [14,15]. Pollen fossils often carry detailed information about the parent plant community, which is direct evidence of past vegetation and environmental evolution. Therefore, pollen analysis has been widely used to reconstruct palaeovegetation and palaeoclimate [16,17]. In addition, as elements are easily brought into lake sediments through biological and abiotic processes [18], their chemical properties are stable and contain a large amount of geological information. Therefore, detailed information about element changes in lacustrine fine-grained sediments is often considered a good indicator for palaeoclimate inversion and reconstruction [19–21]. Over the years, scholars have proven the close correlation between environmental conditions and element abundance in terms of the sources and origins of elements and derived a series of geochemical parameters related to palaeoclimate and the degree of weathering, such as Sr/Cu, Rb/Sr, and Fe/Mn ratios and chemical and plagioclase indices of alteration (CIA and PIA) [22–24]. These parameters provide an important basis for the study of major climatic events in deep time, such as the Neoproterozoic glacial period [25], the Late Triassic Carnian humid event [26], the Early Permian glacial–interglacial transition [27], and the PETM [28].

As a typical Cenozoic basin in southern China, the Pearl River Mouth Basin (PRMB) records harbour geological information stretching back to the Cenozoic; in particular, it has complete sedimentary records of the Eocene. The lacustrine fine-grained sedimentary rocks of the Eocene Wenchang and Enping Formations represent an excellent archive of terrestrial climate conditions during the Eocene and provide an excellent opportunity to reconstruct the Eocene vegetation and climate environment in southern China. Therefore, in this study, we provide detailed sporopollen and elemental geochemical records from the middle-late Eocene strata in the Xijiang main subsag, PRMB, southern China, to reconstruct the climate evolution process in the key geological period of the middle-late Eocene. This study will help deepen the understanding of the continental Eocene climate and environment.

2. Regional Geological Background

The PRMB is located at the northern continental margin of the South China Sea (Figure 1a) with an area of approximately 17.5×10^4 km^2; it is a Cenozoic sedimentary basin developed on a basement of pre-Mesozoic epimetamorphic rocks and Mesozoic granites [29]. It is also an important offshore petroliferous basin in China. Divided by NE-trending and NW-trending basement faults, the PRMB presents a pattern of "north–south zonation and east–west segmentation" (Figure 1b) [30]. It can be further divided into five primary tectonic units and nine secondary tectonic units (Figure 1b) [31].

According to the background and geodynamic analysis of the regional tectonic evolution, the evolution of the PRMB can be divided into four main stages: the prerift stage, rift stage, postrift stage, and tectonic activation stage (Figure 2a) [33]. The basin has a double-layer faulted structure. The Cenozoic strata of the basin consist of the Palaeocene Shenhu Formation, early Eocene Wenchang Formation, late Eocene Enping Formation, Oligocene Zhuhai Formation, Miocene Zhujiang Formation, Hanjiang Formation and Yuehai Formation, and Pliocene Wanshan Formation (Figure 2a). Among them, the Wenchang Formation and Enping Formation belong to the continental sedimentary system, while the Zhuhai Formation, Zhujiang Formation, Hanjiang Formation, Yuehai Formation, and Wanshan Formation belong to the marine sedimentary system [34] (Figure 2a).

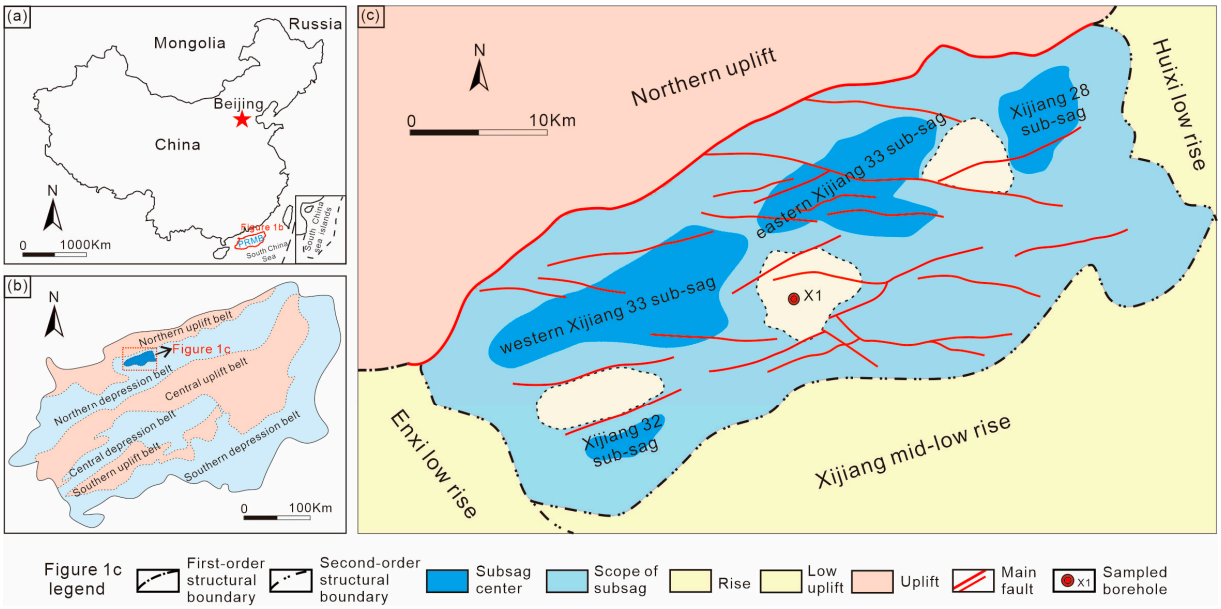


Figure 1. Regional geological map of the study area. (**a**) The location of the Pearl River Mouth Basin; (**b**) the structural outline of the Pearl River Mouth Basin and the location of the study area in the Pearl River Mouth Basin; (**c**) geological map of the study area and sampling drilling location [32].

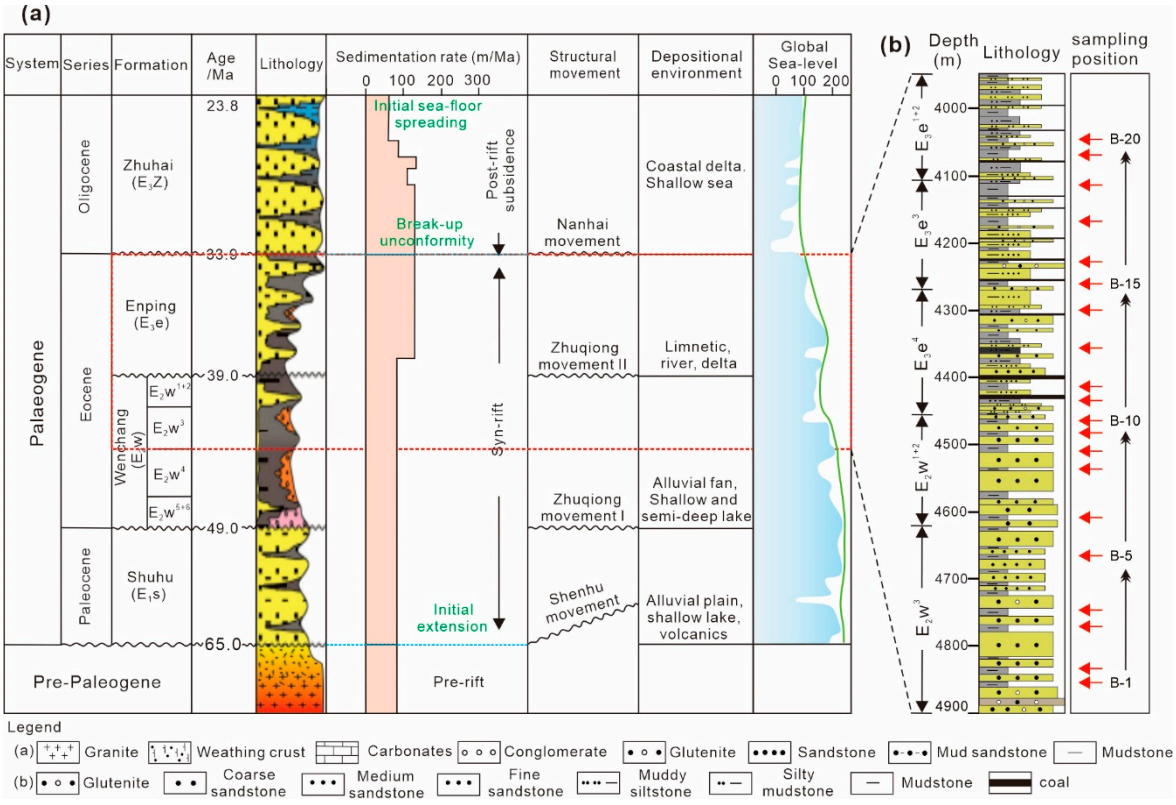


Figure 2. Comprehensive histogram and sampling of Palaeogene strata in the study area. (**a**) Lithostratigraphy, sedimentary environment, and tectonic evolution of the Pearl River Mouth Basin [35–37]; (**b**) Palaeogene lithology histogram of the X1 well and the sampling location.

The main Xijiang subsag (Figure 1b) is located in the western Zhuyi depression in the Pearl River Mouth Basin, bordering the Huizhou sag in the east and the Enping sag in the west. It is within the central and northern uplift zones and has an area of approximately 1100 km^2. The main Xijiang subsag shows a northeast–southwest trend and is mainly

composed of four subsags: the Xijiang 32 subsag, Xijiang 33 west subsag, Xijiang 33 east subsag, and Xijiang 28 subsag (Figure 1c). Among them, the Xijiang 33 west subsag, the Xijiang 33 east subsag, and the Xijiang 28 subsag are controlled by the northern boundary faults, while the Xijiang 32 sag is controlled by the second-level south-dipping faults, and all show a north faulting and south super half-graben structure, down faulting, and up depression [32].

As the target layers of this study, the Wenchang Formation and Enping Formation were limited to the Eocene through the analysis of planktonic foraminifera and calcareous nanofossil samples obtained from ocean drilling and drilling in the PRMB [38,39] combined with the analysis of deep drag geomagnetic anomalies in the northern margin of the South China Sea [40,41]. According to the lithological association and sedimentary environment, the Wenchang Formation can be divided into six sections, and the Enping Formation can be divided into four sections (Figure 2a). The Wenchang Formation is dominated by shallow and semideep lacustrine deposits, and its dark mudstone is one of the important lacustrine source rocks in the PRMB. The Enping Formation mainly features lacustrine, shore-shallow lake and delta plain sedimentary facies. The coal measure strata are also important source rocks for the basin rift period, and the delta plain sand body is an important oil and gas reservoir in the basin. Sampling borehole X1 is one of the few wells drilled in the Wenchang Formation in the Xijiang main sag. It is located in the Xijiang 33 low uplift, and the lake water body was shallow during the sedimentary period of the Eocene Wenchang Formation and the Enping Formation. Delta facies and shore-shallow lake facies were developed, showing the sedimentary characteristics of sand–mud interbeds (Figure 2b).

3. Samples and Experimental Methods

The depth of the X1 well is 4936.5 m. The Wenchang Formation and Enping Formation were drilled in the depth section from 3948 to 4901 m. The Wenchang Formation and Enping Formation are mainly composed of coarse sandstone and mudstone; the environmental information regarding the provenance area was based on these sandstone interbedded sequences, while the reconstruction of the paleoclimate was based on the mudstone. Accordingly, we collected 20 mudstone samples at this depth section, including 10 from the Wenchang Formation and 10 from the Enping Formation (Figure 2b). All 20 samples were tested and analysed for sporopollen and major and trace elements.

The preliminary work of spore-pollen analysis mainly involves washing and filtering. Samples were first soaked in HCl and HF solutions to remove calcium carbonate and siliceous materials, respectively, and the acidified samples were washed and sieved with water to obtain residues containing spores, pollen, planktonic algae, and other organic wall microfossils. The washing and sieving work was usually carried out in an ultrasonic cleaner with a pore size of 10 μm, and the duration was usually less than 2 min. The components larger than 10 μm were concentrated in a test tube to prepare a slide for observation under a transmission light microscope. All the organic wall microfossils in the experimental samples were identified and counted, including spores, pollen, and phytoplankton. The microscope used for identification in this study was a LEICADM4000B biological microscope. The identification and classification of sporopollen species was undertaken following Balme (1995) [42] and Song et al. (1999) [43], and the sporopollen map was drawn using Tilia 2.0 software [44]. The palynoflora zones were divided in the CONISS clustering program using the principle of minimum variance with stratigraphic constraints [45].

Based on the loss on ignition (LOI) data obtained using the traditional calcination technique, lithium tetraborate was used to remove organic matter from the ashed samples. Then, a Philips PW2404 X-ray fluorescence spectrometer was used according to the natural gas industry standard GB/T14506.28-93 for constant element analysis with an analysis error < 5%. To determine trace elements, the powder sample was first digested in an HF-HNO3 acid mixture solution (48 h); the concentrations of trace elements were then determined using inductively coupled plasma–mass spectrometry (ICP–MS) with

spectroscopy (ELEMENT-XR). In this process, the detection temperature was 25 °C, and the relative humidity was 30%. The accuracy of the measurement was ensured by using standard samples and repeated analysis.

4. Results and Interpretation

4.1. Pollen Band Characteristics

The 20 samples in this study contained abundant sporopollen fossils. Among them, there were 37 genera of angiosperms, 20 genera of ferns, and 16 genera of gymnosperms (Figure 3). Abundant algae fossils were observed in some mudstone samples, such as *Pediastrum*, *Gloeocapsomorpha*, and Dinoflagellate.

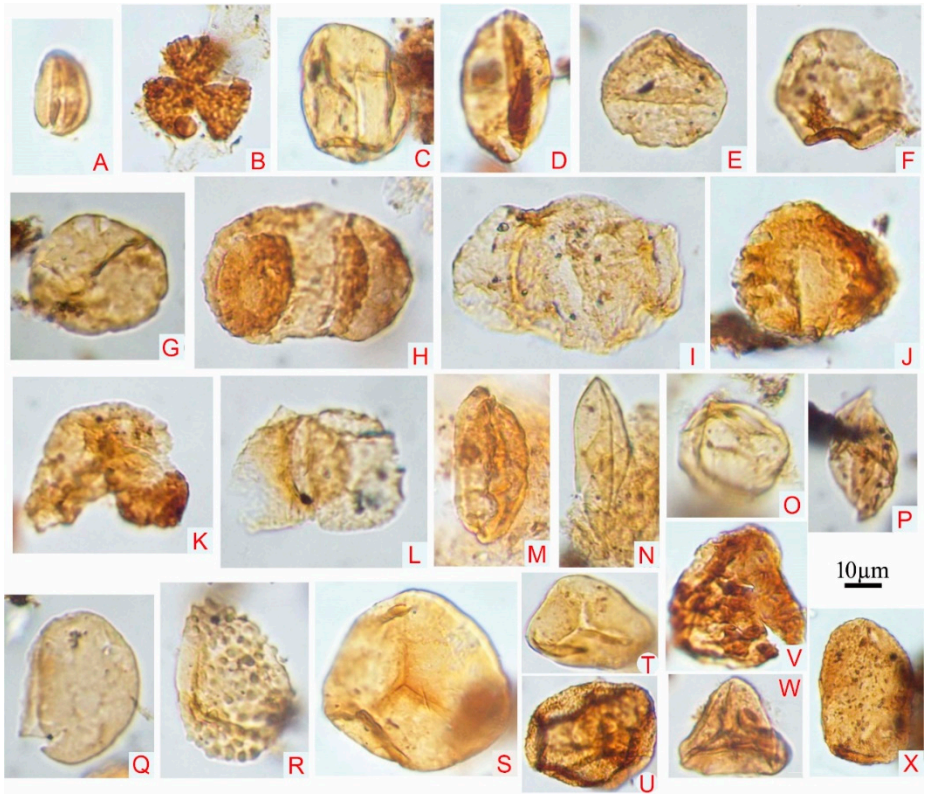


Figure 3. Typical sporopollen fossils from the Wenchang Formation–Enping Formation in the X1 well of the Xijiang main sag. (**A**) *Quercoidites minutus*, (**B**) *Retitricolporites*, (**C**) *Labitricolpites*, (**D**) *Trilobapollis ellipticus*, (**E**) *Ulmipollenites undulosus*, (**F**) *Liquidambarpollenites stigmosus*, (**G**) *Juglanspollenites rotundus*, (**H**) *Abietineaepollenites*, (**I**) *Pinuspollenites labdacus*, (**J**) *Dacrydiumites florinii*, (**K**) *Cedripites minutulus*, (**L**) *Podocarpidites minutus)*, (**M**) *Ephedripites*, (**N**) *Cycadopites acuminatus*, (**O**) *Inaperturopollenites dubius*, (**P**) *Taxodiaceaepollenites*, (**Q**) *Polypodiaceaesporites haardti*, (**R**) *Polypodiisporites usmensis*, (**S**) *Deltoidospora adriensis*, (**T**) *Cyathidites minor Coup*, (**U**) *Osmundacidites* sp., (**V**) *Magnastriatites* sp., (**W**) *Gleicheniidites* sp., (**X**) *Extrapunctatosporis megapunctos*.

The pollen types were mainly angiosperms (4.76%–78.57%). These taxa included *Quercoidites* (maximum abundance: 31.58%), *Retitricolporites* (25.00%), *Tricolpopollenites* (25.00%), *Trilobapollis* (16.67%), *Juglanspollenites* (14.29%), *Liquidambarpollenites* (12.50%), and other pollen (Figure 3).

The gymnosperm pollen type content was 5.14%–73.68%. The genera were *Pinuspollenites* (31.58%), *Cedripites* (28.57%), *Abietineaepollenites* (16.13%), *Podocarpidites* (15.79%), *Tsugaepollenites* (9.09%), *Cycadopites* (8.33%), *Inaperturopollenites* (7.14%), *Piceaepollenites* (4.76%), and *Ephedripites* (4.00%). There was a small amount of *Ginkgo retectina* (0.79%).

The fern spore content was the lowest at 4.35%–62.16%. *Polypodiaceaesporites* (35.14%), *Polypodiisporites* (21.05%), *Extrapunctatosporis* (15.00%), *Osmundacidites* (10.00%), *Deltoi-*

dospora (9.38%), *Gleicheniidites* (9.09%), and *Cyathidites* (8.33%) were the main genera. Small amounts of *Polypodiaceoisporites* (5.26%), *Undula tisporites* (4.05%), *Polypodiaceoisporites*, *Magnastriatites*, etc. (Figure 3) were also present.

Three pollen zones were revealed based on cluster analysis. The characteristics of each zone are described below.

4.1.1. Pollen Zone I

Pollen zone I was dominated by *Quercoidites–Polypodiaceaesporites–Pinuspollenites* (4456–4857 m), including a total of 10 samples. This zone was dominated by angiosperms (4.76%–78.57%), followed by gymnosperms (5.41%–73.68%) and ferns (7.14%–62.16%). Among the angiosperm pollen types, *Quercoidites*, *Retitricolporites*, and *Tricolpopollenites* had the highest contents, followed by *Trilobapollis*, *Juglanspollenites*, and *Liquidambarpollenites*. Among the gymnosperm pollen, *Pinuspollenites* had the highest content, followed by *Abietineaepollenites*, *Podocarpidites*, and so on. Among the fern spores, *Polypodiaceaesporites* and *Polypodiisporites* were the most abundant, followed by *Extrapunctatosporis*, *Osmundacidites*, *Gleicheniidites*, and *Cyathidites* (Figure 4).

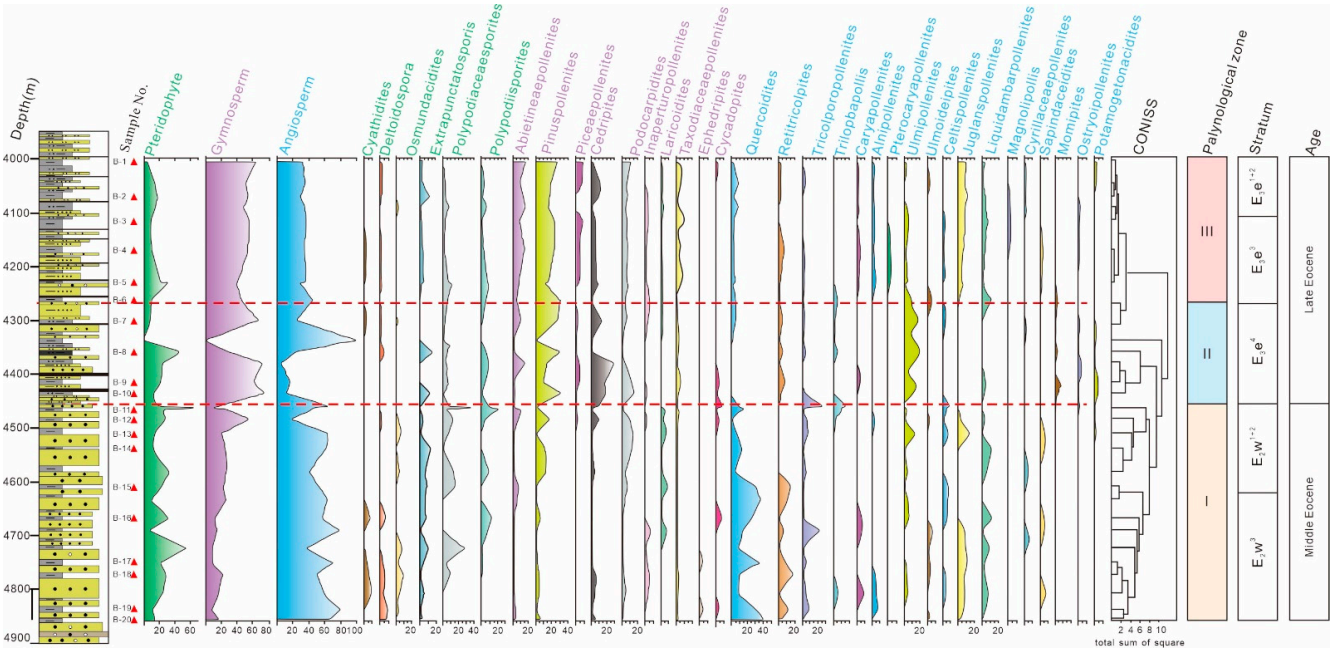


Figure 4. Sporopollen percentage diagram and sporopollen zoning for the Wenchang–Enping Formation in the X1 well of the Xijiang main sag.

4.1.2. Pollen Zone II

Pollen zone II was dominated by *Pinuspollenites–Ulmipollenites–Cedripites* (4268–4456 m), with a total of four samples. The zone was dominated by gymnosperms (45.0%–65.85%), followed by angiosperms (25.61%–45.0%) and fewer ferns (8.54%–10.0%). Among the gymnosperm pollen, *Pinuspollenites* had the highest content, followed by *Cedripites*, *Abietineaepollenites*, *Podocarpidites*, and *Inaperturopollenites*. Among the angiosperm pollen, *Ulmipollenites* and *Liquidambarpollenites* had the highest contents, followed by *Quercoidites*, *Trilobapollis*, *Ulmoideipites*, and *Retitricolporites*. Among the fern spores, small amounts of *Polypodiaceaesporites*, *Polypodiisporites*, *Osmundacidites*, and *Cyathidites* were observed (Figure 4).

4.1.3. Pollen Zone III

Pollen zone III was dominated by the palynofloras of *Pinuspollenites–Abietineaepollenites–Juglanspollenites* (4007–4268 m; Figure 4), with a total of six samples. The zone was domi-

nated by gymnosperms (40.38%–63.77%), followed by angiosperms (28.85%–36.67%) and fewer ferns (4.35%–30.77%). Among the gymnosperm pollen, *Pinuspollenites* had the highest content, followed by *Abietineaepollenites*, *Podocarpidites*, and *Cedripites*. There were many kinds of angiosperm pollen, but the contents were generally low. Among them, *Juglanspollenites* and *Quercoidites* had the highest contents, followed by *Liquidambarpollenites*, *Ulmipollenites*, and *Retitricolporites*. Among the fern spores, *Polypodiaceaesporites* and *Polypodiisporites* had high contents, and small amounts of *Osmundacidites*, *Magnastriatites*, *Deltoidospora*, etc. (Figure 4) were also present.

4.2. Element Geochemical Characteristics

In order to avoid the influence of geochemical factors on the reconstruction of the paleoclimate, only data from the mudstone samples were used. The Sr/Cu ratio was low (3.30–6.02, average: 4.87) in pollen zone I, while the Fe/Mn ratio was higher (67.78–228.20; average: 105.95) (Figure 5). In pollen zone II (En4), the Sr/Cu ratio increased gradually (3.34–10.37; average: 7.76), and the Fe/Mn ratio decreased gradually (37.58–60.95; average: 45.36). In pollen zone III (En3-En1), the Sr/Cu ratio was generally higher (4.82–7.72; average: 6.53); the Fe/Mn ratio was generally low, with high values only at 4069.5 m (39.69–124.02; average: 68.50) (Figure 5). The Al_2O_3 content and Fe/Mn ratio showed consistent trends of change, demonstrating significantly high values in pollen zone I (15.10–24.08; average: 21.32) while pollen zone II (11.18–20.00; average: 14.72) and pollen zone III (9.27–13.00; average: 10.76) showed significant downwards trends (Figure 5).

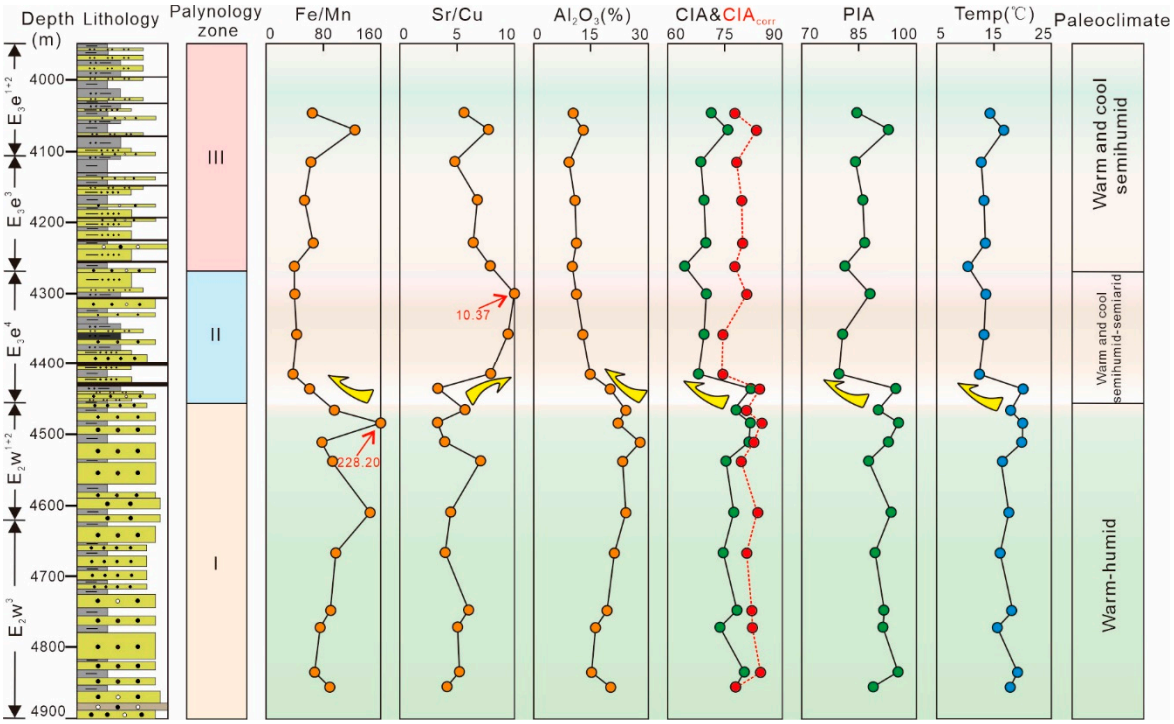


Figure 5. Evaluation of element geochemical parameters for climate and degree of weathering for the middle-late Eocene in the X1 well of the Xijiang main sag.

The formulas for calculating the relevant parameters of the chemical weathering intensity are as follows: (I) chemical alteration index (CIA) = $Al_2O_3/(Al_2O_3 + CaO^* + Na_2O + K_2O) \times 100$ [21,22]; (II) plagioclase alteration index (PIA) = $[(Al_2O_3\text{-}K_2O)/(Al_2O_3 + CaO^* + Na_2O - K_2O)] \times 100$ [23]; (III) $CaO^* = \min(CaO - 10/3 \times P_2O_5, Na_2O)$ [22,46]; (IV) temperature (T) = $0.56 \times CIA - 25.7$ [23]; (V) $CIA_{corr} = [Al_2O_3/(Al_2O_3 + CaO^* + Na_2O + K_2O_{corr})] \times 100$; (VI) $K2O_{corr} = [m \times Al_2O_3 + m \times (CaO^* + Na_2O)]/(1 - m)$; and $m = K2O/(Al_2O_3 + CaO^* + Na_2O + K_2O)$ [47].

In pollen zone I, the CIA and PIA values were higher (CIA: 73.66–81.58; PIA: 87.50–95.36). In pollen zone II, the CIA and PIA values showed decreasing trends (CIA avg.: 72.33; PIA avg.: 85.70). In pollen zone III, the CIA and PIA values were lower (CIA avg.: 69.95; PIA avg.: 85.82). The T value showed a trend consistent with the CIA and PIA values. The average temperature values in pollen zone I, pollen zone II, and pollen zone III were 17.83 °C, 14.80 °C, and 13.47 °C, respectively (Figure 5).

5. Stratigraphic Age Significance of Palynofloras

Numerous *Quercoidites*, *Ulmipollenites*, *Pinuspollenites*, and *Polypodiaceaesporites* appeared in the target interval of this study. *Quercoidites* first appeared in the Late Cretaceous and entered the peak development period after the Eocene, while *Ulmipollenites* is one of the important types of Eocene palynofloras in China [16,48]. Large proportions of *Quercoidites* and *Ulmipollenites* appear to be prominent features of the Eocene palynological face [49,50]. The common drought-resistant *Ephedripites* showed low contents in the Oligocene [15]. The contents of *Picaepollenites* and *Dacrydiimites* were extremely low in this study. Although *Picaepollenites* and *Dacrydiimites* are mostly found in high mountains at an altitude of more than 2500 m [51], they are considered one of the important groups among the Oligocene palynoflora in China, as cold-loving elements were widespread in the Oligocene. Therefore, the palynoflora in this study did not conform to the characteristics of the Chinese Oligocene sporopollen community. Accordingly, the geological age of our palynoflora was likely Eocene.

Previous studies have shown that the Early Eocene palynofloras of China are characterized by the coexistence of porous, tricolpate, and tricolporate types, and the contents of some ancient spores and pollen are low. In the middle Eocene, the tricolpate and tricolporate types of sporopollen tended to flourish and dominate, accompanied by the disappearance of ancient elements [52]. *Pentapollenites* and *Monocolpopollenites tranquillus*, which are common in the early Eocene palynofloras, were absent among the palynofloras of the studied section, and the typical early Eocene ancient spores and pollen *Schizaeoisporites* and *Cicatricosisporites* were not found [52]. This indicated that the palynofloras in this study did not conform to the characteristics of the early Eocene in China. In particular, large proportions of *Retitricolporites* and *Tricolpopollenites* appeared in pollen zone I, which was similar to the dominant palynofloras (*Quercoidites–Tricolpopollenites–Betulaceoipollenites*) found for the middle Eocene in the Fushun Basin, China [15]. However, the palynofloras of the second member of the Liushagang Formation in the Beibu Gulf Basin (*Quercoidites–Ulmipollenites–Pentapollenites*), the third member of the Shahejie Formation in the Bohai Bay Basin (*Quercoidites–Ulmipollenites minor*), and the Dalianhe Formation in the Yilan Basin (*Quercoidites–Taxodiaceaepol–lenites*) all show *Quercoidites* as the dominant type [48,50,53], indicating that the middle Eocene in China was characterized by the massive widespread presence of *Quercoidites*. In addition, zone I also showed that *Quercoidites* was dominant in this study. Combined with the above studies, we concluded that the age of pollen zone I may be middle Eocene.

In pollen zone II, the *Quercoidites* content decreased sharply from 41.8% to 6.10%. The proportions of *Ulmipollenites* and *Pinuspollenites* in zone II increased significantly. Overall, the assemblage of zone II presented the palynoflora characteristics of *Pinuspollenites–Ulmipollenites–Cedripites*, which was consistent with the middle-late Eocene palynofloras in China summarized by Song et al. (1999) [43] and showed high similarity with the late Eocene palynofloras in the beach area of the Huanghua Depression [54]. This suggested that the assemblage of zone II may be attributable to the late Eocene. In addition, in pollen zone III, proportions of cold-resistant elements, such as *Piceaepollenites* and *Taxodiaceaepollenites*, showed increasing trends, and lower amounts of elements characteristic of the Oligocene, such as *Magnastriatites*, appeared. The *Pinuspollenites–Abietineaepollenites–Juglanspollenites* palynofloras can be compared with the palynofloras of the late Eocene in the Fushun Basin [15]. Therefore, it is acceptable that pollen zone III might belong to the late Eocene.

6. Middle-Late Eocene Climate Reconstruction

6.1. Palaeoclimate Indication from Palynology

With the support of the above pollen identification research, we next identified the ancient vegetation types based on the pollen results and then analysed the temperature and humidity types. According to the types of sporopollen and the ecological environment data regarding their genetic types, the spores and pollen in the middle and late Eocene in the study area were divided into coniferous forest, evergreen broad-leaved forest, deciduous broad-leaved forest, shrub, and herb (Table 1) [55,56], and the percentage of each type was calculated. The study of the spores and pollen species in the temperate zone showed that the pollen in the study area could be divided into six types: tropical, subtropical, tropical–subtropical, tropical–temperate, and temperate (Table 1) [14,57]. In addition, the spores and pollen-related parent plants can be divided into four types in accordance with their dry and humid types: xerophytes, mesophytes, hygrophytes, and swamp types (Table 1) [58]. Based on the above classification scheme, a quantitative statistical analysis of the spore and pollen contents for different ecological types in the target interval at the study area was carried out, and the ecological environment characteristics of the parent plants indicated by the sporopollen in the study area were determined. Then, the palaeoclimate evolution process in the study area was predicted.

The early sedimentary period of climate zone I (i.e., pollen zone I) was rich in tropical–subtropical deciduous broad-leaved forests (i.e., *Quercoidites*, *Tricolpopollenites*, etc.). The next most abundant were tropical–temperate coniferous forests (i.e., *Abietineaepollenites*, etc.) and a small number of tropical–subtropical herbs (i.e., *Gleicheniidites* and *Deltoidospora*, etc.) and evergreen broad-leaved forests (i.e., *Cyathidites*, etc.) (Figure 6). In addition, the analysis of dry and humid types showed that most of the pollen was Mesozoic, and the pollen of wet plants comprised a certain proportion of the pollen sampled. Therefore, early climate zone I had a subtropical humid climate (Figure 6). In the late sedimentary period of the climatic zone, the contents of tropical–subtropical deciduous broad-leaved forests, evergreen broad-leaved forests, and herbaceous plants showed decreasing trends among the palynofloras, while the contents of tropical–temperate coniferous forests and herbaceous plants showed significant increasing trends. The vegetation type was coniferous mixed forest, and the increase in the proportion of hygrophytic sporopollen was related to the prosperity of aquatic algae (Figure 6), which may indicate a decrease in palaeotemperature and an increase in humidity in the late period. Therefore, late climate zone I had a warm temperate humid climate.

During the deposition period of climate zone II, compared with climate zone I, the proportions of angiosperms and ferns decreased, while the relative abundance of coniferous forests (i.e., *Pinuspollenites*, *Abietineaepollenites*, *Cedripites*, *Podocarpidites*, etc.) increased significantly and the pollen content indicating deciduous broad-leaved forests (i.e., *Quercoidites*, *Tricolpopollenites*, and *Liquidambarpollenites*, etc.) decreased significantly. Coniferous forests were generally dominant (Figure 6). Tropical–temperate pollen types (*Abietineaepollenites*, *Pinuspollenites*, etc.) showed increasing trends, while tropical elements (*Podocarpidites*, *Cyathidites*, etc.) and tropical–subtropical elements (*Polypodiaceaesporites*, *Quercoidites*, *Tricolpopollenites*, etc.) showed significant downwards trends, suggesting a significant decrease in palaeotemperature during this period. In addition, the decrease in hygrophyte components and the significant increase in swamp components during this period (Figure 6) suggest that the lake base level was shallow (shallow lake and marsh environment). Therefore, climate zone II had a temperate semiarid and semihumid climate.

Table 1. Classification of spore and pollen communities, closest living relatives, vegetation types, temperature zone types, and dry humidity types from the Wenchang–Enping Formation.

Sporopollen	Existing Relative	Vegetation Type	Temperature Zone Type	Dry Humidity Type	Sporopollen	Existing Relatives	Vegetation Type	Temperature Zone Type	Dry Humidity Type
		Angiosperm					Pteridophyte		
Magnolipollis	Magnoliaceae	DBLF	Tro-Sub	Mesophytes	Cyathidites	Cyatheaceae	EBLF	Tropical	Mesophytes
Tricolpopollenites	Hamamelidaceae?	DBLF	Tro-Sub	Mesophytes	Deltoidospora	Polypodiopsida	Herb	Tro-Sub	Hygrophytes
Quercoidites	Quercus	DBLF	Tro-Sub	Mesophytes	Gleicheniidites	Gleicheniaceae?	Herb	Tro-Sub	Hygrophytes
Ulmoideipites	Planera	DBLF	Tro-Sub	Mesophytes	Osmundacidites	Osmundaceae?	Herb	Tro-Tem	Hygrophytes
Rutaceoipollis	Rutaceae	DBLF	Tro-Sub	Mesophytes	Lygodioisporites	Lygodiaceae	Herb	Tro-Sub	Hygrophytes
Cyrillaceaepollenites	Castanea	DBLF	Tro-Tem	Mesophytes	Polypodiaceaesporites	Polypodiaceae	Herb	Tro-Sub	Swamp
Sapindaceidites	Sapindaceae	DBLF	Tro-Sub	Mesophytes			Gymnosperm		
Betulaepollenites	Betulaceae?	DBLF	Temperate	Mesophytes	Abietineaepollenites	Pinus	CF	Tro-Tem	Mesophytes
Momipites	Corylus	Shrub	Temperate	Mesophytes	Pinuspollenites	Pinus	CF	Tro-Tem	Mesophytes
Ostryoipollenites	Ostrya	DBLF	Temperate	Mesophytes	Piceaepollenites	Picea	CF	Temperate	Mesophytes
Caryapollenites	Carya	DBLF	Tro-Sub	Mesophytes	Cedripites	Cedrus	CF	Subtropical	Mesophytes
Alnipollenites	Alnus	DBLF	Temperate	Hygrophytes	Podocarpidites	Podocarpus	CF	Tropical	Hygrophytes
Pterocaryapollenites	Pterocarya	DBLF	Temperate	Hygrophytes	Inaperturopollenites	Taxodiaceae	CF	Subtropical	Swamp
Ulmipollenites	Ulmus	DBLF	Tro-Tem	Mesophytes	Laricoidites	Larix	CF	Tro-Tem	Mesophytes
Celtispollenites	Celtis	DBLF	Tro-Tem	Xerophytes	Taxodiaceaepollenites	Taxodiaceae	CF	Subtropical	Swamp
Juglanspollenites	Juglans	DBLF	Temperate	Mesophytes	Ephedripites	Ephedra	Shrub	Temperate	Xerophytes
Liquidambarpollenites	Liquidambar	DBLF	Tro-Sub	Mesophytes	Cycadopites	Cycadaceae	EBLF	Tropical	Mesophytes
Potamogetonacidites	Potamogeton	Herb	Tro-Tem	Hygrophytes					

DBLF, deciduous broad-leaved forest; EBLF, evergreen broad-leaved forest; CF, coniferous forest; Tro-Sub, tropical–subtropical; Tro-Tem, tropical–temperate.

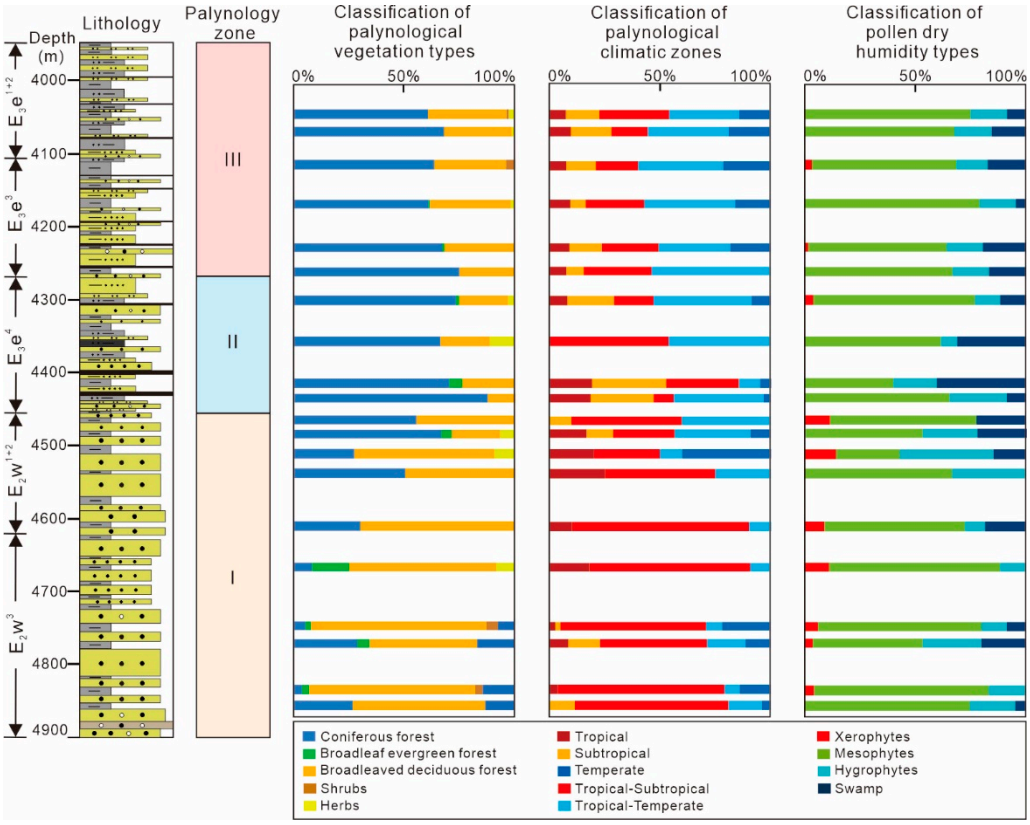


Figure 6. Analysis of the vegetation types, climate types, and dry and humid types revealed by pollen in well X1 of the Xijiang main subsag (lithology legend is shown in Figure 2).

During the sedimentary period of climate zone III, compared with climate zone II, the proportions of tropical–temperate elements (i.e., *Abietineaepollenites*, *Pinuspollenites*, *Osmundacidites*, etc.) and temperate elements (i.e., *Piceaepollenites, Momipites, Ostryoipollenites*, etc.) increased slightly (Figure 6), suggesting that the palaeotemperature rebounded. The indicators of deciduous broad-leaved forests (i.e., *Quercoidites*, *Tricolpopollenites*, etc.) showed increasing trends, while the fern spore content increased further, indicating the slight warming of the climate during this period. In addition, the proportions of mesophytes and hygrophytes further increased, while the proportions of swamp plants decreased (Figure 6), indicating that climate zone III had a warm temperate semihumid climate.

Based on the above analysis of pollen data, climate zone I mainly had a subtropical–warm temperate palaeoclimate in the sedimentary period, climate zone II had a temperate palaeoclimate background, and climate zone III had a warm temperate palaeoclimate.

6.2. Palaeoclimate Indications from Elemental Geochemistry

As good carriers of lake sedimentary information, element ratios are widely used to reconstruct continental palaeoclimates, and various climate indicators have been proposed for the reconstruction of palaeoclimate evolution processes, including Fe/Mn, Sr/Cu, CIA, and PIA [26,59]. Among them, Sr/Cu ratios of 1.3–5.0, 5.0–10.0, and >10.0 usually indicate a warm/humid climate, semihumid–semiarid climate, and cold/arid climate, respectively [59]. As the composition and content of clay minerals show different characteristics under different climatic conditions, the contents of several special main oxides (i.e., SiO_2, Al_2O_3, K_2O, and Na_2O) also show close relationships with the changes in clay minerals. For example, Al_2O_3 is mostly enriched in kaolinite, which is generally related to warm and humid climates, so high Al_2O_3 content is often taken as an indicator of warm and humid climates [60]. Furthermore, a higher Fe/Mn ratio indicates a warm and humid climate, while a lower Fe/Mn ratio is often closely related to a cold and arid climate [61].

Climate zone I was characterized by low Sr/Cu and high Fe/Mn ratios (Figure 5), suggesting warm and humid palaeoclimatic conditions during this period, which may have been related to climate optimization in the middle Eocene [59]. During the sedimentary period of climate zone II, the Sr/Cu ratio increased significantly and the Fe/Mn ratio showed a lower value, indicating that the palaeoclimate began to cool in the late Eocene and transitioned to a warm and cool semihumid–semiarid climate. During the sedimentary period of climate zone III, the ratios of Sr/Cu and Fe/Mn decreased and increased slightly, respectively, compared with those of climate zone II, which indicated that there was slight climate warming in the late Eocene, and the overall climate was cool and semihumid. The trend for the variation in the Al_2O_3 content was consistent with that for the Fe/Mn ratio (Figure 6), both of which reflect consistent palaeoclimatic evolution. The evolution process from climate zone I → climate zone II → climate zone III showed a transition from a warm and humid climate → warm and cool semihumid–semiarid climate → warm and cool semihumid climate (Figure 7a).

In addition, the weathering flux generated by warm and humid climates is significantly greater than that generated by cold and dry climates, which indicates that ancient weathering conditions can reflect the ancient climate environment to a certain extent [62]. At present, the CIA and PIA are widely used to reconstruct palaeoweathering conditions [21,26,59]. Generally, a higher PIA value indicates strong weathering conditions in warm and humid climates, while a CIA value of 80 represents weak, medium, and strong weathering conditions [22]. During diagenesis, metasomatism can significantly change the original element composition of shale (such as potassium), resulting in a low CIA value. Therefore, CIA_{corr} is often combined with the CIA value to comprehensively study ancient weathering conditions [47].

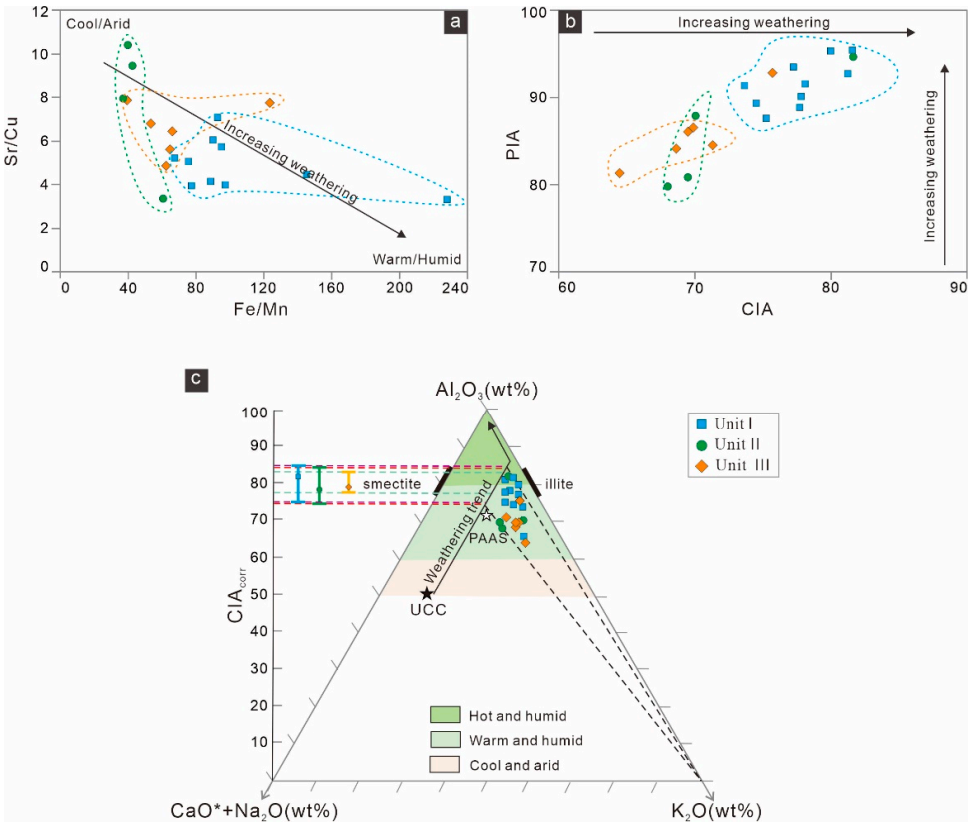


Figure 7. Palaeoclimatic correlation diagram: (**a**) Sr/Cu and Fe/Mn intersection diagram; (**b**) CIA and PIA intersection diagram; (**c**) A–CN–K (Al_2O_3 − CaO * + Na_2O − K_2O) ternary diagram.

The average values for the CIA and CIA_{corr} in climate zone I were 77.73 and 82.81, respectively. The relatively high values indicated that there was strong weathering in this period. Climate zones II and III showed significant decreases in CIA and CIA_{corr}, suggesting the weakening of weathering in the late Eocene (Figure 5), which was related to climate cooling during this period. The PIA value decreased in the order climate zone I > climate zone III > climate zone II, which was consistent with the trends for the CIA and CIA_{corr} curves, indicating that the weathering intensity in the study area decreased in the middle and late Eocene with an accompanying decrease in the degree of wetting (Figure 7b,c), further indicating that the palaeotemperature in the study area gradually decreased, which was also strongly supported by the variation in the temperature values.

In general, climate zone I in the study area was dominated by a warm and humid climate, and the samples from climate zone II were mainly concentrated in the cool semiarid–semihumid area, while the sedimentary period of climate zone III showed a cool semihumid climate, which was basically consistent with the palaeoclimate evolution indicated by the palynology.

7. Middle-Late Eocene Climate Records and Global Climate Evolution

Due to the regulation of high atmospheric pCO_2 in the late Palaeocene and early Eocene, the early Eocene underwent multiple thermal events globally, such as the PETM, ETM, and EECO (Figure 8), which had important impacts on the evolution of global ecosystems and induced a series of biological events, such as mammalian dispersal, benthic extinction, and the emergence of ancient whales [63]. The global climate of the middle Eocene was characterized by inheritance. Although atmospheric pCO_2 showed a decreasing trend over a long period, it remained in a climate condition relatively dominated by greenhouse effects (Figure 8). During this period, the middle Eocene climate optimization (MECO) occurred, characterized by a significant increase in atmospheric pCO_2 and a significant positive shift in marine oxygen isotopes [64]. In Turkey—and even Europe—the sedimentary strata contain abundant spores and pollen, such as *Pliatopollis hungaricus*, *Triporopolenites*, and *Pentapollenites*, which not only have important biostratigraphic significance but also imply that the middle Eocene was a warm and humid climate [65]. Similarly, in eastern Asia, the climate became warm and humid due to the impact of the East Asian monsoon [66]. Correspondingly, *Quercoidites* became dominant over *Ulmipolenites* during the middle Eocene, and several *Ephedra* species associated with drying appeared often, reflecting the existence of a seasonal dry climate during this period [48,50]. The pollen records (dominated by tropical–subtropical vegetation) and geochemical records (high Sr/Cu ratios and high CIA) of climate zone I in the main Xijiang sag also responded to the humid climate of the middle Eocene. In addition, organically rich shale and coal deposits developed widely in the middle Eocene lacustrine basins in eastern and southern China (e.g., the Youganwo Formation in the Maoming Basin, Dalianhe Formation in the Yilan Basin, and Shahejie Formation in the Bohai Bay Basin). These fine-grained sediments are rich in *Quercoidites*, *Ulmipollenites*, and *Tricolpopollenites*, suggesting the dominance of tropical and subtropical sporopollen, which are usually related to the warm and humid climate of the middle Eocene [67–69]. The middle Eocene section of the study area revealed a set of coarse clastic delta deposits (Figure 2b), which may be closely related to the locations of drilling structures and magmatic diapirs, as these accepted more terrestrial debris input. However, in the adjacent Huizhou sag, Lufeng sag, and eastern Yangjiang sag, organically rich shale deposits from the middle Eocene have been shown [59], which were also continental sedimentary responses to global climate optimization in the middle Eocene.

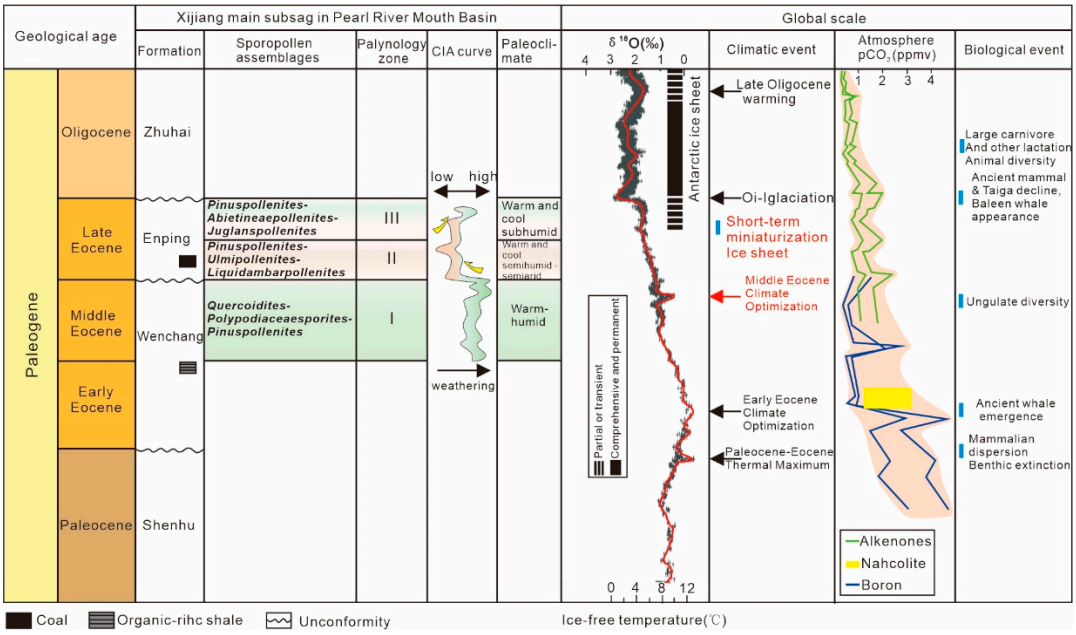


Figure 8. Relationship between global Palaeogene $\delta^{18}O$, palaeotemperature, atmospheric CO_2 concentration, and Palaeogene continental palaeoclimate and sedimentary environment in the study area (oxygen isotopes modified from [63]; ice sheets modified from [70]; CO_2 concentration data follow [63]; and biotic event data follow [71]).

The Pinuspollenites–Ulmipollenites–Liquidambarpollenites palynofloras in climatic zone II of the Xijiang main sag suggest that its age may be late Eocene. During this period, the proportions of angiosperms and ferns decreased, while temperate coniferous forest achieved a dominant position (Figure 6). Additionally, accompanied by a sharp increase in the Sr/Cu ratio and sharp decreases in the CIA and PIA, the climate in the study area rapidly changed from the subtropical humid climate in climate zone I to the temperate semihumid–semiarid climate in climate zone II. This climate change marks a decrease in temperature in the middle/late Eocene, which is consistent with the middle/late Eocene climate cooling event (MLEC) [63]. In the late Eocene, atmospheric pCO_2 and deep-sea oxygen isotopes showed upwards trends, and the polar region showed a partial or transient ice sheet, suggesting a slight recovery of palaeotemperature in the late Eocene. The palynoflora revealed that climate zone III in the study area belonged to the late Eocene. During this period, numbers of tropical–temperate elements rebounded, and the proportions of mesophytes and hygrophytes further increased. The warm temperate semihumid climate of climate zone III corresponds well with the temperature rise in the late Eocene (Figure 8). This correspondence is also strongly supported by elemental geochemical records. Therefore, the palaeoclimate records reflecting the spore-pollen assemblages and element geochemistry of the Xijiang main subsag in the middle-late Eocene Pearl River Mouth Basin show a good coupling relationship with the trend for the changes in global temperature.

8. Conclusions

Through a comprehensive analysis of the palynology and elemental geochemistry of the fine-grained sediments of the Wenchang–Enping Formations in the Xijiang main subsag of the Pearl River Mouth Basin, the climate evolution process in the middle-late Eocene was revealed in detail, and the following conclusions were drawn:

1. A total of 73 genera and 115 species of sporopollen fossils were identified in the Wenchang–Enping Formations, including 37 genera of angiosperms, 20 genera of ferns, and 16 genera of gymnosperms. Palynoflora analysis showed that the Wenchang Formation–Enping Formation could be dated to the middle-late Eocene;

2. The analysis of vegetation type, air temperature type, and the degree of sporopollen dryness and wetness in the target layer of the study area showed that climate zone I mainly had a subtropical–warm temperate palaeoclimate, climate zone II had a temperate palaeoclimate, and climate zone III had a warm temperate palaeoclimate. The palaeoclimate reconstruction results for the element geochemical indicators (Fe/Mn, Sr/Cu, CIA, PIA, etc.) were basically consistent with the palaeoclimatic evolution indicated by palynology;
3. The climate of the middle-late Eocene in the study area showed a transition from a warm and humid climate to a warm and cool semihumid–semiarid climate and then to a warm and cool semihumid climate, demonstrating a good coupling relationship with the trend for the changes in the global temperature.

Author Contributions: Conceptualization, G.P. and X.S.; methodology, W.C. and P.J.; software, M.L. and C.X.; validation, G.P.; formal analysis, G.P.; investigation, G.P., P.J. and M.L.; resources, M.L.; data curation, G.P., Y.H. and C.X.; writing—original draft preparation, G.P.; writing—review and editing, W.C.; visualization, Y.J.; supervision, W.C.; project administration, G.P.; funding acquisition, G.P. All authors have read and agreed to the published version of the manuscript.

Funding: This research was funded by the Significant Science and Technology Project of the 14th Five-Year Plan of the CNOOC "Offshore Deep/Ultra Deep Oil and Gas Exploration Technology", no. KJGG2022-0403.

Data Availability Statement: The data used to support the findings of this study are included within the article.

Acknowledgments: We appreciate the Significant Science and Technology Project of the 14th Five-Year Plan of the CNOOC "Offshore Deep/Ultra Deep Oil and Gas Exploration Technology".

Conflicts of Interest: The authors declare no conflict of interest.

References

1. Miller, K.G.; Fairbanks, R.; Mountain, G.S. Tertiary oxygen isotope synthesis, sea level history, and continental margin erosion. *Paleoceanography* **1987**, *2*, 1–19. [CrossRef]
2. Thomas, E.; Zachos, J.C. Was the late Paleocene thermal maximum a unique event? *GFF* **2000**, *122*, 169–170. [CrossRef]
3. Abels, H.A.; Clyde, W.C.; Gingerich, P.D. Terrestrial carbon isotope excursions and biotic change during Palaeogene hyperthermals. *Nat. Geosci.* **2012**, *5*, 326–329. [CrossRef]
4. Crouch, E.M.; Shepherd, C.L.; Morgans, H.E.G. Climatic and environmental changes across the early Eocene climatic optimum at mid-Waipara River, Canterbury Basin, New Zealand. *Earth-Sci. Rev.* **2020**, *200*, 102961. [CrossRef]
5. Chen, Z.L.; Ding, Z.L. A review on the Paleocene-Eocene Thermal Maximum. *Quat. Sci.* **2011**, *31*, 937–950.
6. Zachos, J.C.; Dickens, G.R.; Zeebe, R.E. An early Cenozoic perspective on greenhouse warming and carbon-cycle dynamics. *Nature* **2008**, *451*, 279–283. [CrossRef]
7. Westerhold, T.; Röhl, U.; Frederichs, T. Astronomical calibration of the Ypresian timescale: Implications for seafloor spreading rates and the chaotic behavior of the solar system? *Clim. Past* **2017**, *13*, 1129–1152. [CrossRef]
8. Korasidis, V.A.; Wallace, M.W.; Wagstaff, B.E. Terrestrial cooling record through the Eocene-Oligocene transition of Australia. *Glob. Planet. Chang.* **2019**, *173*, 61–72. [CrossRef]
9. Teng, X.H.; Wang, C.L.; Shen, L.J.; Wang, J.Y.; Yu, X.C.; Liu, X. Paleoclimate during the Paleocene–Eocene Extreme Thermal Event Recorded by the Deep Drill Core SKD1 in the Jianghan Basin. *Acta Geosci. Sin.* **2022**, *43*, 65–72.
10. Chen, Z.L.; Ding, Z.L.; Tang, Z.H. Early Eocene carbon isotope excursions: Evidence from the terrestrial coal seam in the Fushun Basin, Northeast China. *Geophys. Res. Lett.* **2014**, *5*, 326–329. [CrossRef]
11. Chen, Z.L. Carbon-cycle dynamics during the Paleocene-Eocene Thermal Maximum. *Chin. Sci. Bull.* **2022**, *67*, 1704–1714. [CrossRef]
12. Mosbrugger, V.; Utescher, T.; Dilcher, D.L. Cenozoic continental climatic evolution of Central Europe. *Proc. Natl. Acad. Sci. USA* **2005**, *102*, 14964–14969. [CrossRef]
13. Aleksandrova, G.N.; Kodrul, T.M.; Jin, J.H. Palynological and paleobotanical investigations of Paleogene sections in the Maoming Basin, South China. *Stratigr. Geol. Correl.* **2015**, *23*, 300–325. [CrossRef]
14. Herman, A.B.; Spicer, R.A.; Aleksandrova, G.N. Eocene–early Oligocene climate and vegetation change in southern China: Evidence from the Maoming Basin. *Palaeoecology* **2017**, *479*, 126–137. [CrossRef]
15. Wei, Y.; Yang, B.; Xia, H.D.; Deng, H.J. Paleovegetation and Paleoclimate during Mid-Late Eocene in Fushun Basin. *Earth Sci.* **2021**, *46*, 1848–1861.

16. Wang, X.M.; Wang, M.Z.; Zhang, X.L. Palynology Assemblages and Paleoclimatic Character of the Late Eocene to the Early Oligocene in China. *Earth Sci.* **2005**, *30*, 309–316.
17. Ding, W.J.; Hou, D.J.; Gan, J. Sedimentary geochemical records of late Miocene-early Pliocene palaeovegetation and palaeoclimate evolution in the Ying-Qiong Basin, South China Sea. *Mar. Geol.* **2022**, *445*, 106750. [CrossRef]
18. Algeo, T.J.; Ingall, E. Sedimentary Corg:P ratios, paleocean ventilation, and Phanerozoic atmospheric pO2. *Palaeoecology* **2007**, *256*, 130–155. [CrossRef]
19. Akinlua, A.; Adekola, S.A.; Swakamisa, O. Trace element characterisation of Cretaceous Orange Basin hydrocarbon source rocks. *Appl. Geochem.* **2010**, *25*, 1587–1595. [CrossRef]
20. Yang, H.F.; Zhao, Y.; Cui, Q.Y.; Ren, W.H.; Li, Q. Paleoclimatic indication of X-ray fluorescence core-scanned Rb/Sr ratios: A case study in the Zoige Basin in the eastern Tibetan Plateau. *Sci. Sin. (Terrae)* **2021**, *51*, 73–91. [CrossRef]
21. Xu, C.; Shan, X.L.; He, W.T.; Zhang, K.; Rexiti, Y.; Su, S.Y.; Liang, C.; Zou, X.T. The influence of paleoclimate and a marine transgression event on organic matter accumulation in lacustrine black shales from the Late Cretaceous, southern Songliao Basin, Northeast China. *Int. J. Coal Geol.* **2021**, *246*, 103842. [CrossRef]
22. Nesbitt, H.W.; Young, G.M. Early Proterozoic climates and plate motions inferred from major element chemistry of lutites. *Nature* **1982**, *299*, 715–717. [CrossRef]
23. Fedo, C.M.; Nesbitt, H.W.; Young, G.M. Unraveling the effects of potassium metasomatism in sedimentary rocks and paleosols, with implications for paleoweathering conditions and provenance. *Geology* **1995**, *23*, 921–924. [CrossRef]
24. Xu, J.J. High Resolution Depiction of Organic Matter Accumulation Mechanism in the Upper Cretaceous Oil Shale of the Northern Songliao Basin (NE China). Master's Thesis, Jilin University, Changchun, China, 16 December 2015.
25. Li, W.P.; Li, H.L.; Wang, Y.; Liu, S.F.; Zhang, Z.P.; Yang, W.L.; Cai, X.R.; Qian, T.; Li, X.J. Neoproterozoic glaciations in Yecheng area, southwestern margin of the Tarim Basin. *Earth Sci. Front.* **2022**, *29*, 356–380.
26. Zhang, K.; Liu, R.; Liu, Z.J.; Li, L. Geochemical characteristics and geological significance of humid climate events in the Middle-Late Triassic (Ladinian-Carnian) of the Ordos Basin, central China. *Mar. Pet. Geol.* **2021**, *131*, 105179. [CrossRef]
27. Lu, C.Y. Paleoclimatic Change and Sedimentary Response of the Late Carboniferous-Early Permian in the Basin of Craton in North China Block: A case from the Western Shandong. Master's Thesis, Shandong University of Science & Technology, Qingdao, China, 16 April 2019.
28. Gupta, S.; Kumar, K. Precursors of the Paleocene–Eocene Thermal Maximum (PETM) in the Subathu Group, NW sub-Himalaya, India. *J. Asian Earth Sci.* **2019**, *169*, 21–46. [CrossRef]
29. Sun, X.M.; Zhang, X.Q.; Zhang, G.C.; Lu, B.L.; Yue, J.P.; Zhang, B. Texture and tectonic attribute of Cenozoic basin basement in the northern South China Sea. *Sci. Sin. (Terrae)* **2014**, *44*, 1312–1323. [CrossRef]
30. Xie, H.; Zhou, D.; Li, Y. Cenozoic tectonic subsidence in Deepwater sags in the Pearl River Mouth Basin, northern South China Sea. *Tectonophysics* **2014**, *615–616*, 182–198. [CrossRef]
31. Shi, H.S.; Shu, Y.; Du, J.Y.; Zhu, J.Z. *Petroleum Geology of Paleogene in Zhujiangkou Basin*; Geology Press: Beijing, China, 2017.
32. Liu, P.; Zhang, X.T.; Lin, H.M.; Du, J.Y.; Feng, J.; Chen, W.T.; Liao, J.; Jia, P.M. Distribution Mechanism of Oil and Gas in Xijiang Main Depression of Pearl River Mouth Basin. *J. Jilin Univ. (Earth Sci. Ed.)* **2021**, *51*, 52–64.
33. Hu, Y.; Hao, F.; Zhu, J.Z. Origin and occurrence of crude oils in the Zhu1 sub-basin, Pearl River Mouth Basin, China. *J. Asian Earth Sci.* **2015**, *97*, 24–37. [CrossRef]
34. Mi, L.J.; Zhang, X.T.; Chen, W.T.; Liu, P.; Du, J.Y.; Yao, J.L. Hydrocarbon enrichment law of Paleogene Zhu1 depression and its next exploration strategy in Pearl River Mouth basin. *China Offshore Oil Gas* **2018**, *30*, 1–13.
35. Shi, H.S.; Zhang, X.T.; Chen, W.T.; Liu, P.; Du, J.Y.; Yao, J.L. Hydrocarbon geology, accumulation pattern and the next exploration strategy in the eastern Pearl River Mouth basin. *China Offshore Oil Gas* **2014**, *26*, 11–22.
36. Zhao, F.; Alves, T.M.; Xia, S.H. Along-strike segmentation of the South China Sea margin imposed by inherited pre-rift basement structures. *Earth Planet. Sci. Lett.* **2020**, *530*, 115862. [CrossRef]
37. Haq, B.U.; Hardenbol, J.; Vail, P.R. Chronology of fluctuating sea levels since the Triassic. *Science* **1987**, *235*, 1156–1167. [CrossRef]
38. Li, Q.Y.; Cheng, X.Y.; Chen, J. Data report: Oligocene foraminifers and stable isotopes from IODP Hole U1435A. *Proc. Integr. Ocean. Drill. Program* **2008**, *308*, 1–5.
39. Li, C.F.; Xu, X.; Lin, J.; Sun, Z.; Zhu, J.; Yao, Y.J.; Zhao, X.X. Ages and magnetic structures of the South China Sea constrained by deep tow magnetic surveys and IODP Expedition 349. *Geochem. Geophys. Geosystems* **2014**, *15*, 4958–4983. [CrossRef]
40. Wang, P.X.; Jian, Z.M. Exploring the deep South China Sea: Retrospects and prospects. *Sci. China Earth Sci.* **2019**, *62*, 1473–1488. [CrossRef]
41. Lin, J.; Li, J.B.; Xu, Y.G.; Sun, Z.; Zhou, Z.Y. Ocean drilling and major advances in marine geological and geophysical research of the South China Sea. *Acta Oceanol. Sin.* **2019**, *41*, 125–140.
42. Balme, B.E. Fossil in situ spores and pollen grains: An annotated catalogue. *Rev. Palaeobot. Palynol.* **1995**, *87*, 81–323.
43. Song, Z.C.; Zheng, Y.H.; Li, M.Y. Fossil spores and pollen of China. In *The Late Cretaceous and Tertiary Spores and Pollen*; Science Press: Beijing, China, 1999; pp. 1–770.
44. Grimm, E.C. *Tilia and Tiliagraph*; Illinois State Museum: Springfield, IL, USA, 1991.
45. Grimm, E.C. CONISS: A FORTRAN 77 program for stratigraphically constrained cluster analyses by the method of incremental sum of squares *1. *Comput. Geosci.* **1987**, *13*, 13–35. [CrossRef]
46. McLennan, S.M. Weathering and global denudation. *J. Geol.* **1993**, *101*, 295–303. [CrossRef]

47. Panahi, A.; Young, G.M.; Rainbird, R.H. Behavior of major and trace elements (including REE) during Paleoproterozoic pedogenesis and diagenetic alteration of an Archean granite near Ville Marie, Qu'ebec, Canada. *Geochim. Cosmochim. Acta* **2000**, *64*, 2199–2220. [CrossRef]
48. Xia, X.F.; Zhang, Y.; Yu, J.X.; Yi, C. Eocene-Oligocene palynology and biostratigraphic correlation in the Nanpu Sag, Bohai Bay Basin, -North China. *Acta Micropalaeontologica Sin.* **2015**, *32*, 269–284.
49. Tao, M.H.; Wang, K.F.; Zheng, G.G.; Zhi, C.Y. Early Tertiary sporopollen assemblages from Jizhong Depression and their stratigraphic implication. *Acta Micropalaeontol. Sin.* **2001**, *18*, 274–292.
50. Xie, J.Y.; Li, J.; Mai, W.; Zhang, H.L.; Cai, K.L.; Liu, Y. Palynofloras and age of the Liushagang and Weizhou Formations in the Beibuwan Basin, Sounth China Sea. *Acta Palaeontol. Sin.* **2012**, *51*, 385–394.
51. Hao, X.; Weng, C.; Huang, C.; Ouyang, X. Mid-Late Miocene vegetation and environments in Southeast China: Insights from a marine palynological record in northwestern Taiwan. *J. Asian Earth Sci.* **2017**, *138*, 306–316. [CrossRef]
52. Song, Z.C.; Liu, G.W. Old Tertiary sporopollen assemblages in northeastern Xizang and their paleogeographic significance. In *Paleontology of Xizang*; Part 5; Science Press: Beijing, China, 1982; pp. 165–190.
53. Liu, M.L. Upper Cretaceous and Tertiary Palyno-assemblage sequences in Northeast China. *J. Stratigr.* **1990**, *14*, 277–285.
54. Zhang, T. Sporopollen assemblages from the Palaeogene in the Tanhai area of Haunghua Depression, and their PaIaeoclimate anaIysis. Master's Thesis, Northwest University, Xi'an, China, 2004.
55. Guo, X.; Wang, D.; Ding, X.; Zong, W.; Zhou, W. Early–Middle Cretaceous sporopollen assemblages and new progress on biogeography in the Northern Part of Tarim Basin. *Geol. Rev.* **2011**, *57*, 870–880.
56. Xu, Z.; Li, J.; Zhu, Q.; Li, H.; Zeng, H.; Wei, J.; Zhang, B.; Cao, M.; Hong, B. Early Cretaceous spore and pollen assemblage from the Yixian Formation in the Qianjiadian Depression, Kailu Basin and its paleoclimate implications. *Geol. China* **2021**, *48*, 1924–1934.
57. Chumakov, N.M.; Zharkov, M.A.; Herman, A.B.; Doludenko, M.P.; Kalandadze, N.M.; Lebedev, E.L.; Ponomarenko, A.G.; Ratian, A.S. Climatic belts of the mid-Cretaceous time. *Stratigr. Geol. Correl.* **1995**, *3*, 241–260.
58. Mendes, M.M.; Dinis, J.L.; Gomez, B.; Pais, J. Reassessment of the cheirolepidiaceous conifer Frenelopsis teixeirae Alvin et Pais from the Early Cretaceous (Hauterivian) of Portugal and paleoenvironmental considerations. *Rev. Palaeobot. Palynol.* **2010**, *161*, 30–42. [CrossRef]
59. Xu, C.; Shan, X.L.; Lin, H.M.; Hao, G.L.; Liu, P.; Wang, X.D.; Shen, M.R.; Rexiti, Y.; Li, K.; Li, Z.S.; et al. The formation of early Eocene organic-rich mudstone in the western Pearl River Mouth Basin, South China: Insight from paleoclimate and hydrothermal activity. *Int. J. Coal Geol.* **2022**, *253*, 103957. [CrossRef]
60. Moradi, A.V.; Sari, A.; Akkaya, P. Geochemistry of the Miocene oil shale (hançili formation) in the Çankırı-Çorum basin, Central Turkey: Implications for paleoclimate conditions, source–area weathering, provenance and tectonic setting. *Sediment. Geol.* **2016**, *341*, 289–303. [CrossRef]
61. Reheis, M.C. Influence of climate and eolian dust on the major-element chemistry and clay mineralogy of soils in the northern Bighorn Basin, U.S.A. *Catena* **1990**, *17*, 219–248. [CrossRef]
62. Kasting, J.F. The goldilocks planet? How Silicate Weathering Maintains Earth "Just Right". *Elements* **2019**, *15*, 235–240. [CrossRef]
63. Zachos, J.; Pagani, M.; Sloan, L. Trends, rhythms, and aberrations in global climate 65Ma to present. *Science* **2001**, *292*, 686–693. [CrossRef]
64. Pearson, P.N.; Van Dongen, B.E.; Nicholas, C.J. Stable warm tropical climate through the Eocene Epoch. *Geology* **2007**, *35*, 153. [CrossRef]
65. Akgün, F. Stratigraphic and Paleoenvironmental significance of Eocene Palynomorphs of Corum-Amasya area in the central Anatolia, Turkey. *Acta Palaeontol. Sin.* **2002**, *41*, 576–591.
66. An, Z.S. Late Cenozoic climate change in Asia: Loess, monsoon and monsoon-arid environment evolution. In *Developments in Paleoenvironmental Research*; Springer: Amsterdam, The Netherlands, 2014; p. 16.
67. Xie, X.M.; Li, M.W.; Littke, R. Petrographic and geochemical characterization of microfacies in a lacustrine shale oil system in the Dongying Sag, Jiyang Depression, Bohai Bay Basin, eastern China. *Int. J. Coal Geol.* **2016**, *165*, 49–63. [CrossRef]
68. Xu, C.; Hu, F.; Meng, Q.T.; Liu, Z.J.; Shan, X.L.; Zeng, W.R.; Zhang, K.; He, W.T. Organic Matter Accumulation in the Y ouganwo Formation (Middle Eocene), Maoming Basin, South China: Constraints from Multiple Geochemical Proxies and Organic Petrology. *ACS Earth Space Chem.* **2022**, *61*, 1653–1670.
69. Ping, S.F. Research of Paleoenvironment Process during the Eocene in Yilan area of Yi-Shu Graben. Master's Thesis, Jilin University, Changchun, China, 2020.
70. Francis, J.E. A 50-Million-Year-Old Fossil Forest from Strathcona Fiord, Ellesmere Island, Arctic Canada: Evidence for a Warm Polar Climate. *Arct. Inst. N. Am.* **1988**, *41*, 314–318. [CrossRef]
71. Lawver, L.A.; Gahagan, L.M. Opening of Drake Passage and its impact on Cenozoic ocean circulation. *Oxf. Monogr. Geol. Geophys.* **1998**, *39*, 212–226.

Disclaimer/Publisher's Note: The statements, opinions and data contained in all publications are solely those of the individual author(s) and contributor(s) and not of MDPI and/or the editor(s). MDPI and/or the editor(s) disclaim responsibility for any injury to people or property resulting from any ideas, methods, instructions or products referred to in the content.